



## Detection efficiency evaluation for low energy of a NaI(Tl) scintillation detector

Seongjin Maeng <sup>a,\*</sup>, Sang Hoon Lee <sup>a,b</sup>, Seong Jin Park <sup>a,c</sup>, Woo Cheol Choi <sup>d,e</sup>

<sup>a</sup> School of Energy Engineering, Kyungpook National University, Daegu, 41566, South Korea

<sup>b</sup> Radiation Science Research Institute, Kyungpook National University, Daegu, 41566, South Korea

<sup>c</sup> Korea Foundation of Nuclear Safety, Seongnam, Gyeonggi-do, 13493, South Korea

<sup>d</sup> Department of Radiology, Daegu Catholic University, Hayang-Eup, Gyeongsan, Gyeongbuk, 38430, South Korea

<sup>e</sup> BRNC, Geumcheon-gu, Seoul, 08507, South Korea



### ARTICLE INFO

#### Keywords:

NaI(Tl) scintillation detector

X-ray escape

Low energy range

Detection efficiency

### ABSTRACT

To improve the characterization of the detection efficiency of a NaI(Tl) scintillation detector in the low energy range, measurements and Monte Carlo simulations were performed with a certified reference material (CRM) and disk sources. The detection efficiency was modeled. In the MCNP simulation, the detection efficiency dropped as expected at 33.17 keV. The X-ray escape correction factors of a <sup>204</sup>Tl disk source and MCNP simulations were compared, a factor of the <sup>204</sup>Tl was similar. Moreover, Correcting the X-ray escape and using fewer sources than the CRM resulted in better detection efficiency for the NaI(Tl) detector in the low energy range.

## 1. Introduction

The thallium doped sodium-iodide (NaI(Tl)) scintillation detector was developed by Robert Hofstadter in 1948; it is used worldwide in different radiation research fields including cosmic-ray detection, basic particle study, limited in-situ monitoring for nuclide identification, environmental monitoring, dose evaluation, education, and training. The NaI(Tl) scintillation detector used in gamma-ray spectrometry has a range of sizes; it is robust enough to withstand environmental effects such as physical impacts and temperature; moreover, it can identify gamma-ray energies such as a high purity germanium radiation detector (Bagatelas et al., 2010; Cecchini et al., 2003; Han et al., 2020; Hung et al., 2016; Khodyuk et al., 2010).

These radiation spectrometers are calibrated to identify gamma-rays and radionuclides between 0 and 3 MeV; their detection efficiencies are routinely evaluated with certified reference materials (CRMs) with different geometries, such as 50, 450, and 1000 ml Marinelli beakers. The detection efficiency of these detectors is influenced by self-absorption based on the sample mass density, random summing effects, true coincidence summing effects, X-ray escape from detector materials, and other factors (Deepa et al., 2021; El-Khatib et al., 2014, 2017). To analyze spectra accurately, these effects should be corrected (Li et al., 2016; Meyerhof and West, 1954). For instance, true coincidence summing effects must be corrected for accurate radionuclide

evaluation and validation (De Felice et al., 2000); because that the true coincidence summing effects in CRM analysis can hinder the evaluation of the absolute detection efficiency. To mitigate these effects in the low energy range, researchers have studied the use of external-radiation shield material (copper) (Byun, 2018). In addition, the use of NaI(Tl) scintillation detectors for radiation analysis can be hindered in the low energy range because of poor energy resolution and X-ray escape from detector materials.

In this study, to improve the detection efficiency of a NaI(Tl) scintillation detector in the low energy range, measurements and Monte Carlo simulations were performed with a CRM and disk sources. The NaI (Tl) scintillation detector was calibrated to extend the peak energy range of the spectra for radiation analysis. The iodine X-ray escape correction factors were calculated with Monte Carlo simulations. In addition, the corrected detection efficiencies for iodine X-ray escape from the spectrometer were evaluated.

## 2. Materials and methods

### 2.1. Experiment with NaI(Tl) scintillation detector

A 3 × 3 inch NaI(Tl) scintillation detector with a photomultiplier tube (Alpha spectra, Inc., positive high voltage), a photomultiplier tube base (PMT; ORTEC 266), an amplifier (ORTEC 672; 1 μs shaping time), a

\* Corresponding author.

E-mail address: [todaysmsj@hotmail.com](mailto:todaysmsj@hotmail.com) (S. Maeng).

multi-channel analyzer (ORTEC ASPEC-927; 2<sup>14</sup> channel), and a power supply (ORTEC 566; 800 V) were used for the radionuclide measurements with a lead shield (ORTEC G-5). MAESTRO was used with a job control function to collect data (AMETEK, 2008). The photomultiplier tube was supplied with +800 V. Moreover, the signal amplifier gains of the amplifier were adjusted to enable radiation measurements between 10 keV and 3 MeV.

A CRM (450 ml Marinelli beaker; agar; density: 1 g cm<sup>-3</sup>; uncertainty: from 4.0% to 4.2%) from the Korea Research Institute of Standards and Science was measured to calibrate the detector. The CRM includes <sup>241</sup>Am (595 keV), <sup>109</sup>Cd (88.0 keV), <sup>57</sup>Co (122.1 and 136.5 keV), <sup>139</sup>Ce (165.9 keV), <sup>113</sup>Sn (391.7 keV), <sup>85</sup>Sr (514 keV), <sup>137</sup>Cs (662 keV), <sup>88</sup>Y (898 and 1836.1 keV), and <sup>60</sup>Co (1173.2 and 1332.5 keV). In addition, <sup>137</sup>Cs, <sup>133</sup>Ba, <sup>22</sup>Na, <sup>60</sup>Co, and <sup>204</sup>Tl disk sources (1 µBq; RSS8; Spectrum Techniques; ±20% uncertainty) were separately measured to analyze the measurement spectra and to evaluate the detection efficiency of the NaI(Tl) scintillation detector. The measurements took 1 h for disk sources each disk sources and 3 h for the CRM. The measurement system is depicted in Fig. 1. Multiple-peak analysis was conducted with a multiple-peak fitting function of OriginPro 2021 (OriginLab, USA) (OriginLab Corporation and All, 2022). The multiple-peaks analyzing function is executed step by step. In the first step, the peak analyzing modes is selected (i.e., a single peak or multiple peaks). In the second step, the background is determined (i.e., a linear or a polynomial expression). In the leas step, the peak function is chosen. Finally, the multiple-peaks analyzer analyzes the selected peak of the spectrum.

The detection efficiency (cps Bq<sup>-1</sup>) was evaluated with Equation (1). In addition, the multi-log polynomial function in Equation (2) was used as a fitting function to evaluate the detection efficiency (Gilmore, 2008; Glenne F. Knoll, 2000);

$$\varepsilon = \frac{C}{A I_r T F_X F_T} \quad (1)$$

$$\ln(\varepsilon) = \sum_{i=0}^n a_i \ln(E)^i \quad (2)$$

where  $C$  is the net count of each peak,  $A$  the radioactivity (Bq),  $I_r$  the photon emission ratio of the radionuclide;  $T$  the measuring time (s);  $F_X$  a variable for the correction of iodine X-ray escape from the detector,  $F_T$  a time correction factor (such as the short half-life of the radionuclide or dead time correction). In equation (2),  $E$  is the energy (keV).  $a_i$  fitting constants, and  $n$  the maximum degree of freedom for the fit. The X-ray escape correction factors of each peak were evaluated with Equation (3);

$$F_X = \frac{C}{C + C_{\text{X-ray}}} \quad (3)$$

where  $C_{\text{X-ray}}$  denotes the count of X-ray escape peaks of each peak.

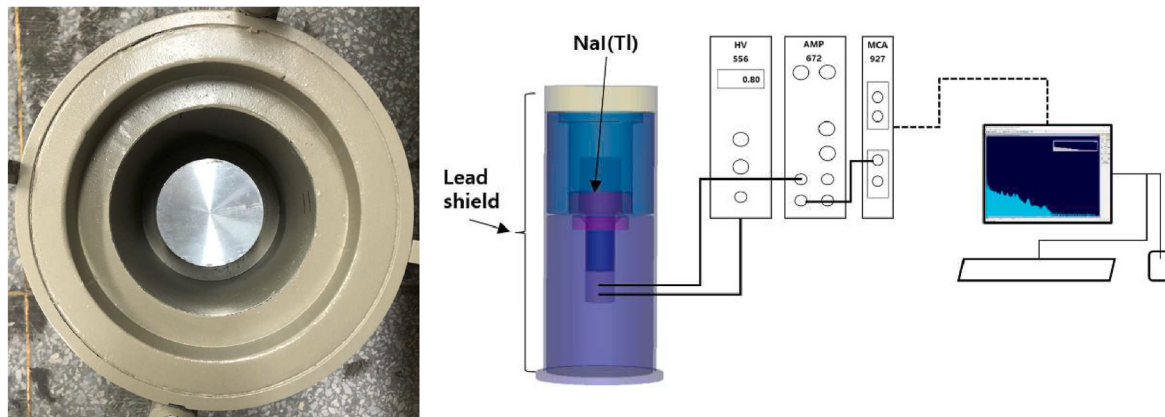


**Fig. 1.** Detection system with G-5 shield for NaI(Tl) scintillation detector.

## 2.2. Monte Carlo simulation

The Monte Carlo N-particle radiation transport code (MCNP6 Beta, Los Alamos National Laboratory, USA) was used to simulate the detection efficiency of the NaI(Tl) detector system. The main parameters of the Monte Carlo simulation are listed in Table 1. For example, the NaI (Tl) crystal density was 3.667 g cm<sup>-3</sup> and the density of the reflector (MgO) was 2.2 g cm<sup>-3</sup>. In particular, the photomultiplier tube in the NaI (Tl) scintillation detector consisted of glass, gas (He), and metal (Cu). The inner gas in the PMT was assumed to be a vacuum because of either the low density or low helium partial pressure inside the tube (Hakamata et al., 2007). The PMT copper density was 8.96 g cm<sup>-3</sup>. Moreover, the MCNP simulation geometries of the NaI(Tl) scintillation detector, 450 ml Marinelli beaker, X-ray image of the detector, and disk sources are shown in Fig. 2.

In the Monte Carlo simulation, photon and electron modes, a source generation function (SDEF), and the F8 tally (i.e., the energy deposition count tally) of the MCNP were used. In addition, to apply the full width at half maximum (FWHM) of the NaI(Tl) scintillation detector, a Gaussian energy broadening technic (i.e., the GEB option) was used;

$$\text{FWHM} = a + b\sqrt{E + cE^2} \quad (4)$$

where FHWM is represented in MeV;  $E$  is the energy (MeV) of a photon, and  $a$ ,  $b$ , and  $c$  are constants estimated from experimental results (Han et al., 2020; Werner et al., 2017). In this study, data from both the disk sources and CRM were used for the GEB option. The FWHMs of the NaI (Tl) scintillation detector showed similar trends regardless of the source geometries. For example, the energy resolution values (i.e., the FWHM per peak energy) at the 662 keV peak were  $6.3 \pm 0.33\%$  (disk source) and  $6.9 \pm 0.35\%$  (CRM). The fitting results ( $a$ ,  $b$ ,  $c$ ) and the coefficient of determination ( $R^2$ ) of Equation (4) were 0 MeV, 0.03328 MeV<sup>1/2</sup>, 0.9572 MeV<sup>-1</sup>, and 0.975, respectively. The measurement uncertainties of the detection efficiency in this study were below 2% based on the Poisson statistical distribution; however, the uncertainty of each

**Table 1**  
Parameters of simulated geometry.

Components	Elements or Compounds	Density (g cm <sup>-3</sup> )
Scintillation Material	NaI	3.667
Reflector	MgO	2.0
Housing	Al	2.702
Polyethylene	H, C, O	0.96
PMT		
-Metal	Cu	8.96
-Glass	SiO <sub>2</sub>	2.2
-Gas	He	0

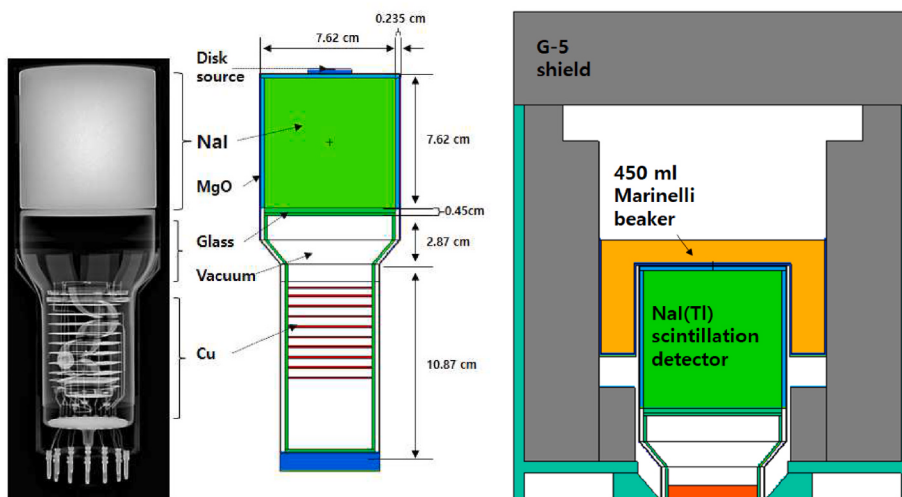


Fig. 2. X-ray image and MCNP geometry of NaI(Tl) scintillation detector.

detection efficiency was included in the manufactory's radioactivity uncertainty.

### 3. Results and discussion

#### 3.1. Energy correction

The radionuclides of the CRM measurement identified with the energy calibrated NaI(Tl) scintillation detector are shown in Fig. 3 (a). In the low energy range, there were energy peaks of radioisotopes ( $^{109}\text{Cd}$ ,  $^{137}\text{Cs}$ , et al.) at  $22 \pm 0.9$  and  $32 \pm 4.5$  keV; in addition, there was  $50 \pm 1.3$  keV with unknown origin. It is unknown whether the 50 keV peak is a random sum peak of  $^{113}\text{Sn}$  X-rays (approximately 24 and 27 keV) or due to iodine X-ray escape associated with  $^{109}\text{Cd}$  (88 keV). Furthermore, the power function for the channel to energy calibration can explain the energy of the low energy peaks better than the linear function, as shown in Fig. 3 (b).

In this study, X-X or X-gamma-ray coincidence summing effects of a  $^{133}\text{Ba}$  disk source measurement result of the NaI(Tl) scintillation detector were identified in the low energy range (Jonsson et al., 2020). The summed or overlapped peaks of identified X-rays and gamma-rays of the  $^{133}\text{Ba}$  source in the NaI(Tl) scintillation detector were presented as shown in Fig. 4 and Table 2 (Bé et al., 2004b). In the energy calibration with disk sources ( $^{22}\text{Na}$ ,  $^{60}\text{Co}$ , and  $^{137}\text{Cs}$ ), the power function could identify the peak energy more effectively than the linear function, as shown in the  $^{133}\text{Ba}$  spectrum. The calibration results are shown in

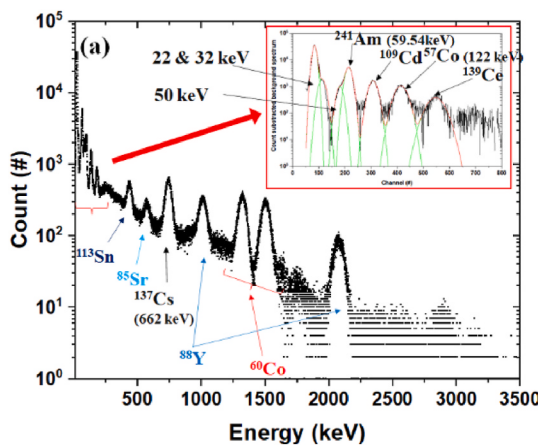


Fig. 3. (a) Measured spectrum of CRM and (b) comparison of energy calibration methods.

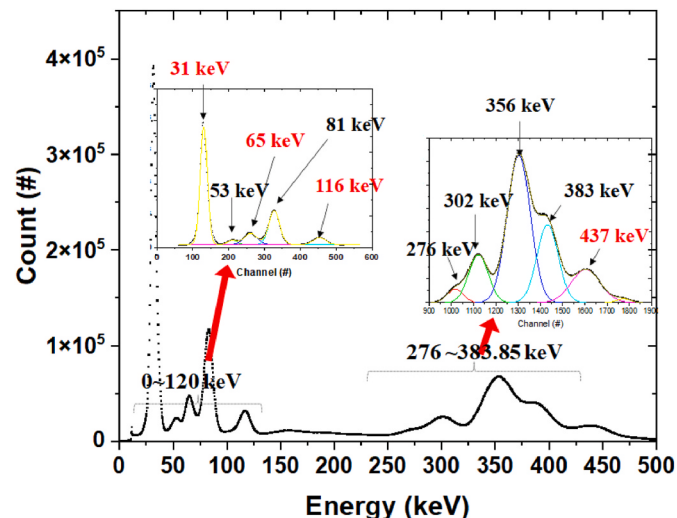
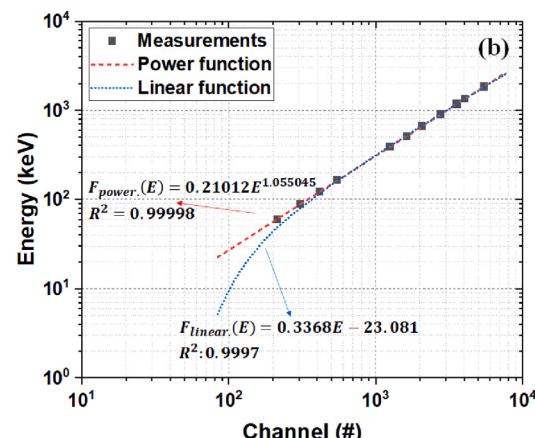


Fig. 4. Measurement spectrum and multiple-peak analysis (red color represents coincidence summing peaks) of  $^{133}\text{Ba}$  disk source.

Table 2. The overlapped peaks were analyzed with the multiple-peak analysis function considering the FWHM. For example, a calculated peak at approximately channel 130 could be identified as a 31.7 keV



**Table 2**

Comparison of results of each energy calibration method with  $^{133}\text{Ba}$  disk source (asterisks denote peaks of summed or overlapped peaks).

Energy (keV)	Channel-to-energy calibration			etc.
	Channel	Power (keV)	Linear (keV)	
$\approx 31.7^*$	130.8	31.7	26.6	$K_{\alpha}$ or $K_{\beta}$
53.2	210.6	52.2	49.5	Gamma
$\approx 65.9^*$	261.6	65.5	64.2	$K_{\alpha}+K_{\beta}$
81.0	327.3	82.9	83.1	Gamma
$\approx 113^*$	453.5	116.7	119.4	$K_{\alpha}$ or $K_{\beta} + 81$ keV
276.4	1017.4	272.1	281.5	Gamma
302.9	1121.6	301.3	311.4	Gamma
356.0	1302.9	352.6	363.5	Gamma
383.9	1432.8	389.5	400.9	Gamma
$\approx 437^*$	1604.5	438.5	450.2	Full energy

peak because of the X-ray summing effect [for example,  $K_{\alpha}$  (approximately 30.1 keV) and  $K_{\beta}$  (approximately 35 keV)] (Bé et al., 2004b).

The detection efficiency of the photons emitted by  $^{133}\text{Ba}$ , was difficult to evaluate because the combined coincidence summing effect and iodine X-ray escape. The detection efficiency of the 53 keV peak was evaluated without considering the coincidence summing effect. Therefore, the measurement data of the  $^{133}\text{Ba}$  source were excluded from the detection efficiency analysis and fit.

### 3.2. Detection efficiency of 450 ml CRM

The detection efficiency for the NaI(Tl) scintillation detector for the CRM is shown in Fig. 5. The coincidence summing effects of each gamma-ray emitted by  $^{60}\text{Co}$  and  $^{88}\text{Y}$  were corrected with the detected summing peaks for the evaluation of the detection efficiency. An expected edge occurred in the detection efficiency at 33.17 keV in Monte Carlo simulation; it is due to the K-shell binding energy of iodine in a NaI (Tl) scintillation crystal (Berger et al., 2010; Gilmore, 2008). In addition, peaks at  $22 \pm 0.9$  and  $50 \pm 1.3$  keV were identified with multiple-peak analysis; however, their detection efficiencies were not calculated because the photon-emitting radionuclide could not be determined. The detection efficiency of 32 keV X-ray from  $^{137}\text{Cs}$  was  $0.155 \pm 0.012$  cps  $\text{Bq}^{-1}$  when only  $^{137}\text{Cs}$  X-ray emission was considered and  $0.107 \pm 0.025$  cps  $\text{Bq}^{-1}$  after the correction of X-rays and gamma-rays from the other radionuclides;  $^{113}\text{Sn}$  (approximately 27.5 keV),  $^{241}\text{Am}$  (approximately 26 keV), and  $^{139}\text{Ce}$  (approximately 33 keV). Therefore,  $3.758 \pm 0.003$

keV FWHM was assumed for the energy of interest.

The detection efficiencies in the low energy range were evaluated based on the fitted results of the CRM and the Monte Carlo simulation, as shown in Fig. 5. Considering the FWHMs of each peak, this difference can be explained based on the probability that the 59.5 keV peak of  $^{241}\text{Am}$  could be combined with the iodine X-ray escape peak of  $^{109}\text{Cd}$  (88.0 keV); moreover, the 88.0 keV peak of  $^{109}\text{Cd}$  can be combined with an iodine X-ray escape peak (approximately 89.4 keV) and a backscattering peak (approximately 83 keV) of 122.6 keV ( $^{57}\text{Co}$ ); the 122.6 keV peak of  $^{57}\text{Co}$  can be combined with a peak escaped iodine X-ray (approximately 137 keV) of 165.9 keV ( $^{139}\text{Ce}$ ); and the 165.9 keV of  $^{139}\text{Ce}$  can be combined with a back-scattering peak (approximately 170 keV) of 514 keV ( $^{85}\text{Sr}$ ). These radionuclides, which affect each other in a CRM, can be un-useful for evaluating the detection efficiency of NaI(Tl) scintillation detectors.

### 3.3. Detection efficiencies of disk sources

In the  $^{22}\text{Na}$ ,  $^{60}\text{Co}$ , and  $^{137}\text{Cs}$  disk sources, the X-rays emitted by  $^{22}\text{Na}$  and  $^{60}\text{Co}$  were not detected because they are below the low energy detection threshold of the detector; Nevertheless, the true coincidence summing peaks (1786 and 2505 keV) of gamma-rays emitted by the radionuclides can clearly be identified in Fig. 6 (a) and (b). The detection efficiencies of these radionuclides were evaluated and corrected with the net count of coincidence summing peaks. The annihilation radiation (ANN) of a background spectrum was subtracted from the detected  $^{22}\text{Na}$  spectrum to calculate the 511 keV peak count. The detection efficiencies of 511 and 1274.5 keV peaks of  $^{22}\text{Na}$  were  $0.157 \pm 0.031$  and  $0.064 \pm 0.013$  cps  $\text{Bq}^{-1}$ , respectively. Moreover, the detection efficiencies of the 1173 and 1332 keV peaks of  $^{60}\text{Co}$  were  $0.083 \pm 0.017$  and  $0.071 \pm 0.014$  cps  $\text{Bq}^{-1}$ , respectively. The detection efficiency of the 662 keV  $^{137}\text{Cs}$  was  $0.127 \pm 0.025$  cps  $\text{Bq}^{-1}$ . Such as in other studies, an X-ray peak ( $K_{\alpha}$ : approximately 31.8 and approximately 32.2 keV;  $K_{\beta}$ : approximately 36.3 and approximately 37.3 keV) of  $^{137m}\text{Ba}$  after  $^{137}\text{Cs}$  decay was detected (M.-M. Be et al., 2006; MEHTA et al., 1987; Ukaegbu and Gamage, 2018). The detection efficiency of the X-ray peak in the disk source was  $0.225 \pm 0.045$  cps  $\text{Bq}^{-1}$ .

The  $^{204}\text{Tl}$  disk source was analyzed individually to collect data of a measurement without the effect of X-ray escape (approximately 72 keV) of lead. The  $^{204}\text{Tl}$  photon emission peaks are at 68.9 keV ( $I_{\gamma}: 0.00474$ ), 70.8 keV ( $I_{\gamma}: 0.00812$ ), and 79.8–80.7 keV ( $I_{\gamma}: 0.00273$ ) (Bé et al., 2004a). The peaks at 70.6 and 81 keV overlapped, as shown in Fig. 6 (d). The peaks were analyzed using the multiple peak analyzers. In addition, an X-ray escape peak was detected at approximately 40 keV; it occurred in the measurement spectrum and the MCNP simulation result of the  $^{204}\text{Tl}$  disk source. This escape peak has an offset of approximately 30 keV from the main photon peak (Salgado et al., 2012). The calculated detection efficiency of the evaluated peak (70.6 keV) was  $0.287 \pm 0.057$  cps  $\text{Bq}^{-1}$ , and the detection efficiency corrected by the X-ray escape effect was  $0.328 \pm 0.058$  cps  $\text{Bq}^{-1}$ .

### 3.4. Comparison of X-ray escape ratios

X-ray escape primarily affects the spectroscopic analysis; results in the photoelectric absorption range of NaI(Tl) scintillation detectors (Salgado et al., 2012). In this study, the X-ray escape correction factors for the range 40–836 keV was calculated with MCNP simulations with the GEB option for both disk sources and the 450 ml CRM, as shown in Fig. 7. The iodine X-ray escape peak (approximately 41 keV, Fig. 6 (d)) was due to the escape of iodine  $K_{\alpha}$  (approximately 28 keV) and  $K_{\beta}$  (approximately 33.2 keV) X-rays with their energies subtracted from the 70 keV gamma-ray emission peak of  $^{204}\text{Tl}$ . The calculated X-ray escape correction factors for the 70.6 keV peak from the  $^{204}\text{Tl}$  disk source were  $0.89 \pm 0.02$  (measurement); and  $0.89 \pm 0.01$  (MCNP simulation). Although the disk sources and the 450 ml Marinelli beaker had different geometries, the X-ray escape correction factors were similar for both

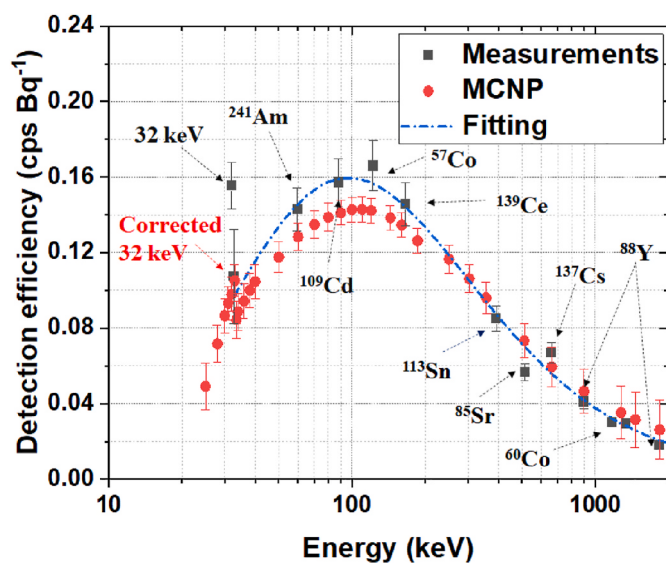
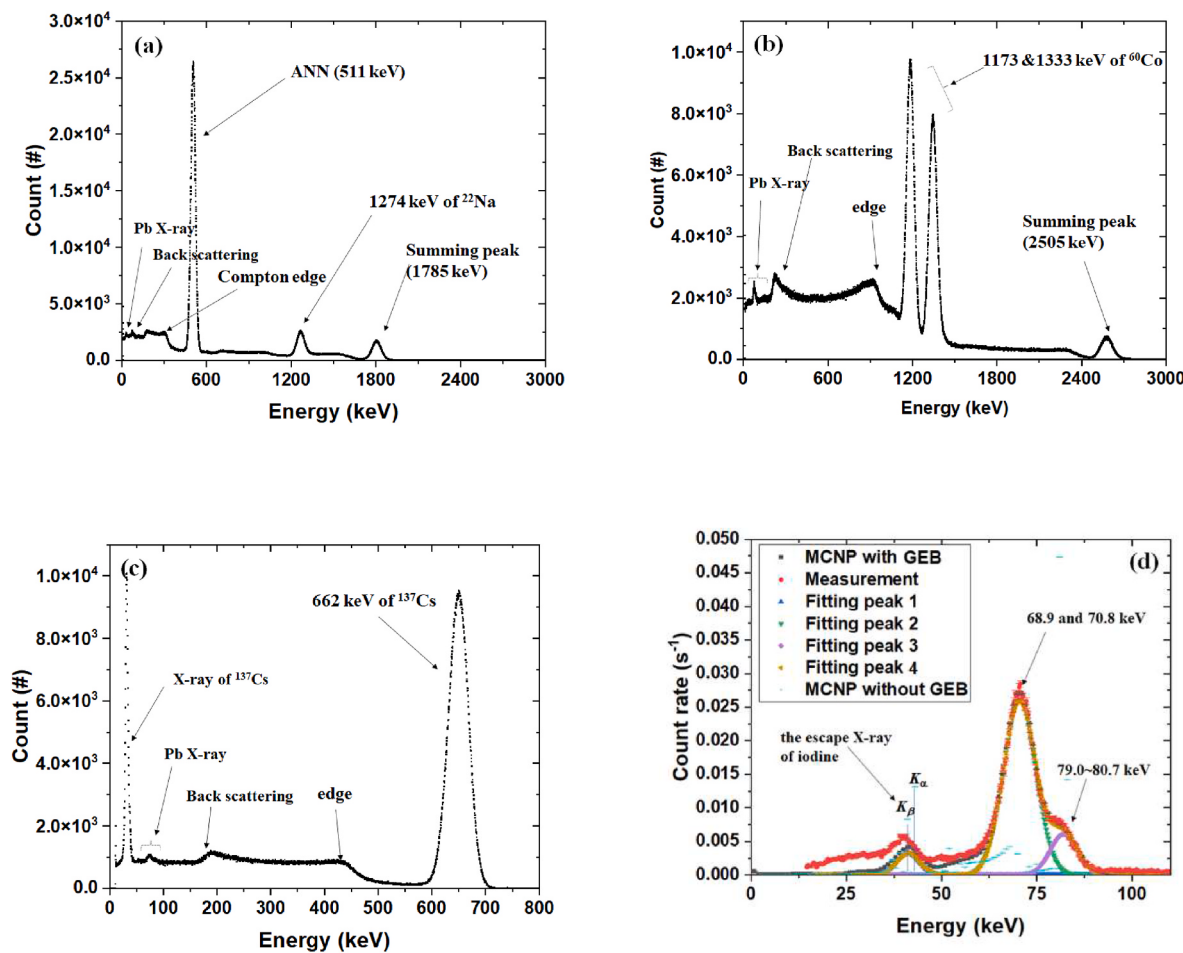
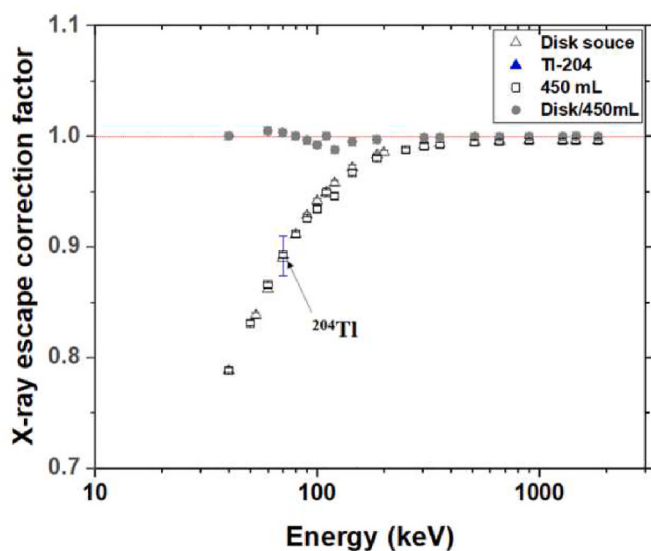


Fig. 5. Detection efficiency of CRM with NaI(Tl) scintillation detector (measurement, fitting results, and MCNP simulation).

Fig. 6. Measurement spectra: (a)  $^{22}\text{Na}$ , (b)  $^{60}\text{Co}$ , (c)  $^{137}\text{Cs}$ , and (d)  $^{204}\text{Tl}$ .Fig. 7. Iodine X-ray escape correction factors for NaI(Tl) scintillation detector based on MCNP simulation, and  $^{204}\text{Tl}$  (measurement).

sources. In fact, they had a linear relationship with a slope of 0.997; and an intercept of 0.004. This fit results in an  $R^2$  of 0.996. Overall, from 40 to 1836 keV, the X-ray escape correction factors for the disk sources ranged from  $0.79 \pm 0.01$  to  $1.00 \pm 0.01$ . Above 120 keV, the correction

factor exceeded 0.958.

### 3.5. Detection efficiency correction with disk sources

The detection efficiencies for the disk sources were estimated via curve fitting with nonlinear regression and seven data points. The measured detection efficiencies without X-ray escape were naturally similar to the fitting results, as shown in Fig. 8 (a). However, in energy differencing detection efficiency, such as 45, 220, and 1460 keV, the discrepancy between the MCNP and fitting results was 18.92%, 11.23%, and 6.78%, respectively. In the disk sources, the difference between fitting results based on the corrected detection efficiency and MCNP simulation results was 0.04% (32.7 keV), 0.42% (70.1 keV), 1.94% (511 keV), 2.85% (661.65 keV), 6.18% (1173 keV), 6.62% (1274 keV), and 2.01% (1333 keV), as shown Fig. 8 (b). When the X-ray escape effect at 45, 220, and 1460 keV peaks was corrected, the difference in the detection efficiency between the MCNP simulation and the fitting results was reduced to 2.47%, 1.51%, and 0.41%, respectively. The fitted detection efficiency with corrected X-ray escape agreed better with the MCNP simulation results than in the non-corrected case, particularly, in the low energy range, as shown in Fig. 8 (b).

In general spectroscopic measurements with NaI(Tl) scintillation detectors, peaks in the low energy range are not analyzed because the analysis of the detection efficiency is complicated (Grujić et al., 2013). With a certified reference source that has a suitable number of radionuclides with gamma-ray peak energies that are reasonably separated such as  $^{241}\text{Am}$  (88 keV) and  $^{139}\text{Ce}$  (165 keV), the calibration of NaI(Tl) scintillation detectors is relatively straightforward (Ji et al., 2019; Salgado et al., 2012). Furthermore, the results of this study show that the

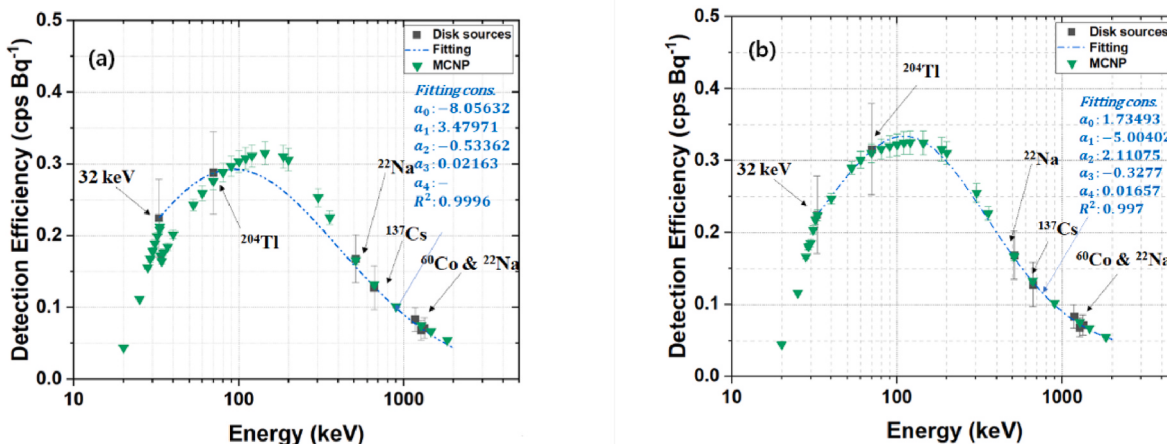


**Fig. 8.** Detection efficiency evaluated with MCNP, fitted measurement results, and disk source data: (a) before X-ray escape correction, (b) after X-ray escape correction.

use of  $^{137}\text{Cs}$  X-rays (32 keV) extends the calibration energy range; more specifically, the energy range of interest is extended to lower values.

#### 4. Conclusions

The aim of this study was to improve the detection efficiency and extend the working range of a  $3 \times 3$  inch NaI(Tl) scintillation detector in the low energy range. In order to achieve this, the detection efficiencies of the NaI(Tl) scintillation detector in the low energy range, were evaluated in measurements and MCNP simulations with 450 ml CRM and disk sources.

As expected, the detection efficiency edge due to the X-ray escape effect occurred at approximately 33.2 keV. In the measurement results of the CRM and the disk sources, the contributions of the iodine X-ray escape, and coincidence summing effects were observed; the detection efficiency was corrected by corrections factors. To improve the evaluation of the low energy detection efficiency, the detection efficiency of the emission X-rays of  $^{137}\text{Cs}$  of the measurement results was added for the fit.

If a CRM contains many nuclides, the detection efficiency evaluation or calibration in the low energy range may be inaccurate owing to various interactions; this effect is evident in the CRM measurement results in this study. To avoid this problem, reducing the number of nuclides and using emission X-rays of use nuclides could be better in the detection efficiency evaluation.

An additional study with other CRM Marinelli beaker sizes and different nuclides will be conducted to validate the presented analysis method. Nevertheless, we believe that the results of this study can be helpful for the analysis of the low energy range.

#### Author statement

**Seongjin Maeng:** Conceptualization, Methodology, Formal analysis, Investigation, Data curation, Writing-Original draft preparation, Writing-Reviewing and Editing, **Sang Hoon Lee:** Writing- Reviewing and Editing, **Seong Jin Park:** Resources, Investigation, **Woo Cheol Choi:** Resources, Investigation.

#### Declaration of competing interest

The authors declare that they have no known competing financial interests or personal relationships that could have appeared to influence the work reported in this paper.

#### References

- AMETEK, 2008. MAESTRO-32 Software User's Manual, A65-B32. AMETEK, Advanced Measurement Technology, Inc.
- Bagatelas, C., Tsabarlis, C., Kokkoris, M., Papadopoulos, C.T., Vlastou, R., 2010. Determination of marine gamma activity and study of the minimum detectable activity (MDA) in 4pi geometry based on Monte Carlo simulation. Environ. Monit. Assess. 165, 159–168. <https://doi.org/10.1007/s10661-009-0935-4>.
- Bé, M.-M., Chisté, V., Dulieu, C., Browne, E., Chechev, V., Kuzmenko, N., Helmer, R., Nichols, A., Schönfeld, E., Dersch, R., 2004a. Table of Radionuclides. Vol. 2 - A = 151 to 242).
- Bé, M.-M., Chisté, V., Dulieu, C., Chechev, V., Kuzmenko, N., Helmer, R., Nichols, A., Schönfeld, E., Dersch, R., 2004b. Table of Radionuclides. Bureau International Des Poids Et Mesures (BIPM) (Vol. 1 - A = 1 to 150).
- Be, M.-M., Chiste, V., Dulieu, C., Browne, E., Baglin, C., Chechev, V., Kuzmenko, N., Helmer, R., Kondev, F., MacMahon, D., Lee, K.B., 2006. Table of Radionuclides (Vol.3 - A = 3 to 244), Monographie BIPM-5.
- Berger, M.J., Hubbell, J.H., Seltzer, S.M., Chang, J., Coursey, J.S., Sukumar, R., Zucker, D.S., Olsen, K., 2010. XCOM: Photon Cross Sections Database, vol. 8. <https://doi.org/10.18434/T48G6X> [WWW Document]. NIST Stand. Ref. Database.
- Byun, J.-I., 2018. A copper shield for the reduction of X-ray true coincidence summing in gamma-ray spectrometry. J. Radiat. Prot. Res. 43, 137–142. <https://doi.org/10.14407/jrpr.2018.43.4.137>.
- Cecchini, S., Galli, M., Giovannini, G., Longo, G., Pagliarin, A., 2003. Real-time monitoring of environmental radiation in Tunguska (Siberia). J. Geophys. Res. Atmos. 108 <https://doi.org/10.1029/2002jd002417>.
- Corporation, OriginLab, All, 2022. Fitting multiple peaks with the multiple peak fit tool [WWW Document]. URL <https://www.originlab.com/doc/Origin-Help/Fit-Multi-PeakFit-Tool>.
- De Felice, P., Angelini, P., Fazio, A., Biagini, R., 2000. Fast procedures for coincidence-summing correction in  $\gamma$ -ray spectrometry. Appl. Radiat. Isot. 52, 745–752. [https://doi.org/10.1016/S0969-8043\(99\)00239-0](https://doi.org/10.1016/S0969-8043(99)00239-0).
- Deepa, S., Vijay Sai, K., Rao, D.R., Madhusudhana Rao, K., Venkataramanah, K., 2021. EC-decay of  $^{133}\text{Ba}$  revisited by electron-gamma spectroscopy. J. of Radioanal. Nucl. Chem. 328 (3), 1001–1010.
- El-Khatib, A.M., Thabet, A.A., Elzaher, M.A., Badawi, M.S., Salem, B.A., 2014. Study on the effect of the self-attenuation coefficient on  $\gamma$ -ray detector efficiency calculated at low and high energy regions. Nucl. Eng. Technol. 46, 217–224. <https://doi.org/10.5516/NET.04.2013.077>.
- El-Khatib, A.M., Salem, B.A., Badawi, M.S., Gouda, M.M., Thabet, A.A., Abbas, M.I., 2017. Full-Energy peak efficiency of an NaI(Tl) detector with coincidence summing correction showing the effect of the source-to-detector distance. Chin. J. Phys. 55, 478–489. <https://doi.org/10.1016/j.cjph.2016.11.013>.
- Gilmore, G.R., 2008. Practical Gamma-Ray Spectrometry, second ed. WILEY.
- Grujić, S., Dorčević, I., Milošević, M., Kozmidis-Luburić, U., 2013. Monte Carlo simulation of GM probe and NaI detector efficiency for surface activity measurements. Radiat. Meas. 58, 45–51. <https://doi.org/10.1016/j.radmeas.2013.08.002>.
- Hakamata, T., Kume, H., Okano, K., Tomiyama, K., Kamiya, A., Yoshizawa, Y., Matsui, H., Otsu, I., Taguchi, T., Kawai, Y., Tamagushi, H., Suzuki, K., Suzuki, S., Morita, T., Hamamatsu Photonics, K., 2007. Photomultiplier Tubes: Basics and Applications, 3rd ed. K. Electron Tube Division.
- Han, S.Y., Maeng, S., Lee, H.Y., Lee, S.H., 2020. Preliminary study on the detection efficiency and estimation of minimum detectable activity for a NaI(Tl)-based seawater monitoring system. J. Environ. Radioact. 218, 106222 <https://doi.org/10.1016/j.jenvrad.2020.106222>.
- Hung, N.Q., Chuong, H.D., Vuong, L.Q., Thanh, T.T., Tao, C., Van, 2016. Intercomparison NaI(Tl) and HPGe spectrometry to studies of natural radioactivity on geological

- samples. J. Environ. Radioact. 164, 197–201. <https://doi.org/10.1016/j.jenvrad.2016.07.035>.
- Ji, Y.Y., Jang, M., Lee, W., 2019. Development of the environmental radiation survey program and its application to in situ gamma-ray spectrometry. Health Phys. 116, 840–851. <https://doi.org/10.1097/HP.0000000000001043>.
- Jonsson, S., Kastlander, J., Vidmar, T., Ramebäck, H., 2020. Experimental validation of corrections factors for  $\gamma$ - $\gamma$  and  $\gamma$ -X coincidence summing of  $^{133}\text{Ba}$ ,  $^{152}\text{Eu}$ , and  $^{125}\text{Sb}$  in volume sources. J. Radioanal. Nucl. Chem. 323, 465–472. <https://doi.org/10.1007/s10967-019-06938-3>.
- Khodyuk, I.V., Rodnyi, P.A., Dorenbos, P., 2010. Nonproportional scintillation response of NaI:Tl to low energy x-ray photons and electrons. J. Appl. Phys. 107, 113513. <https://doi.org/10.1063/1.3431009>.
- Knoll, Glenne F., 2000. Radiation Detection and Measurement, Third. ed. Jpen Wiley & Sons, Inc.
- Li, Liqian, Alexander, Quincy, van der Ende, Bryan, 2016. A method for coincidence summing compensation of simulation results using mcnp on Co60 volume source. CNL Nucl. Rev. 1–5. <https://doi.org/10.12943/CNR.2015.00053>.
- Mehta, D., Singh, S., Verma, H.R., Singh, N., Trehan, P.N., 1987. X- and gamma-ray intensity measurements in  $^{137}\text{Cs}$  and  $^{203}\text{Hg}$  decays. Nucl. Instrum. Methods Phys. Res. A 254, 578–582.
- Meyerhof, W.E., West, H.I., 1954. Note on the escape peak correction for NaI(Tl) crystals. Rev. Sci. Instrum. 25 <https://doi.org/10.1063/1.1770905>, 1025–1025.
- Salgado, C.M., Brandão, L.E.B., Schirru, R., Pereira, C.M.N.A., Conti, C.C., 2012. Validation of a NaI(Tl) detector's model developed with MCNP-X code. Prog. Nucl. Energy 59, 19–25. <https://doi.org/10.1016/j.pnucene.2012.03.006>.
- Ukaegbu, I., Gamage, K., 2018. A model for remote depth estimation of buried radioactive wastes using CdZnTe detector. Sensors 18, 1612. <https://doi.org/10.3390/s18051612>.
- Werner, C.J., Armstrong, J., Brown, F.B., Bull, J.S., Casswell, L., Cox, L.J., Dixon, D., Forster, R.A., Goorley, J.T., Hughes, H.G., Favorite, J., Martz, R., Mashnik, S.G., Rising, M.E., Solomon, C., Sood, A., Sweezy, J.E., Werner, Christopher J., Zukaitis, A., Anderson, C., Elson, J.S., Durkee, J.W., Johns, R.C., McKinney, G.W., McMath, G.E., Hendricks, J.S., Pelowitz, D.B., Prael, R.E., Booth, T.E., James, M.R., Fensin, M.L., Wilcox, T.A., Kiedrowski, B.C., 2017. MCNP User's Manual Code Version 6.2. Los Alamos National Laboratory.